






Performance of Chain Energy-Absorbing Anti-Impact Brackets

Like Zhao¹, Xueqi Zhang¹, Hao Luo^{2*}, Hanjun Gao³, Xinpin Zhang¹, Shuwei Hu¹,
Yonghui Xiao², Runze Zhang³

¹ Inner Mongolia Yitai Group Company Limited, Ordos 010300, China

² Faculty of Information, Liaoning University, Shenyang 110000, China

³ School of Civil Engineering, North China University of Technology, Beijing 100000, China

Corresponding Author Email: luohao8711@163.com

Copyright: ©2025 The authors. This article is published by IETA and is licensed under the CC BY 4.0 license (<http://creativecommons.org/licenses/by/4.0/>).

<https://doi.org/10.18280/ijssse.150309>

ABSTRACT

Received: 9 January 2025

Revised: 12 February 2025

Accepted: 22 March 2025

Available online: 31 March 2025

Keywords:

chain anti-impact hydraulic support, energy-absorbing elements, rockburst, tunnel support, numerical simulation, mine safety

With the continuous increase in mining depth, conventional portal support systems have demonstrated insufficient resistance to dynamic impacts, posing significant safety challenges. To address this issue, a novel multi-directional chain-type anti-impact hydraulic support is proposed. The design integrates specially shaped induced slots within the top beam and incorporates flexible chain support structures on both sides to enhance structural resilience. The proposed support structure achieves a 38.5% increase in energy absorption efficiency without significant changes in its overall dimensions. A series of multi-directional impact load simulations were conducted to investigate the deformation characteristics, failure-prone regions, and overall support performance, using equivalent plastic strain and vertical displacement as key evaluation metrics. The principal findings are as follows: (1) Under vertical impact loading, the equivalent plastic strain is primarily concentrated at the mid-joint of the top beam, identifying it as the most vulnerable region. Reinforcement of this area is recommended in future structural designs. For low-velocity lateral impacts, the strain localizes at the connection between the flexible chain and the bracket, suggesting the addition of a ring base at this location, which improves its resistance to localized rockburst damage. (2) The three hydraulic columns exhibit non-uniform vertical displacements under vertical impact, indicating a suboptimal load-bearing response. This uneven deformation reveals a tendency for the central region to fail under concentrated loads. (3) The induced slot demonstrates velocity-sensitive deformation behavior—smaller under high-speed impacts and larger under low-speed impacts—indicating an inherent responsiveness that enables timely activation of energy-dissipation mechanisms during the early stages of a rockburst. (4) While the lateral impact resistance of the flexible chain structure is slightly lower than its vertical performance, it remains effective in preventing asymmetric failure propagation, thereby enhancing roadway stability under complex stress conditions.

1. INTRODUCTION

The short-term rockburst prediction in underground engineering plays a significant role in the safety of the workers and equipment [1-4]. As a major coal-producing and consuming country, rockbursts are frequent in China [5, 6]. Due to the massive mining of shallow coal resources, which has been gradually depleted, the form of coal mining has shifted towards deep mining [7, 8]. As mining depth increases, mining safety challenges become more technical and structural in nature, requiring enhanced support systems to adapt to dynamic load environments.

As the mining depth continues to increase, the surrounding rock conditions become increasingly complex and variable, and the elastic energy accumulated in the coal and rock mass increases significantly [9]. This leads to a greater possibility of rockburst events, which can result in severe accidents [10, 11], causing heavy casualties and substantial economic losses.

It has been found that more than 90% of rockbursts occur in the roadway, so roadway support has become a critical focus in the research of rockburst prevention and control.

Traditional supports, especially portal-type hydraulic structures, often fail to accommodate complex impact scenarios, leading to reduced energy absorption efficiency and insufficient lateral restraint. The main methods of roadway support in China include anchor cables, U-beams, and hydraulic supports. Hydraulic support is commonly used for roadways with strong impact hazards and is generally regarded as a rigid support under dynamic loads [12-16]. However, this rigid structure is often insufficient to ensure the stability of the support system and the integrity of surrounding rock during impact events. As mining depths increase, U-shaped steel arches have also revealed problems of inadequate load-bearing capacity. Enhancing the impact resistance of hydraulic supports has become one of the essential methods for preventing and controlling rockburst disasters [17-19].

To address this problem, Vardoulakis [20] analyzed the surface instability of a semi-infinite layer of cohesive-frictional material under plane-strain uniaxial compression. Ma et al. [21] and Pan et al. [22] studied the influence of support stiffness and damping on roadway support under rockburst by establishing a dynamic support model. Nevertheless, the current structural forms of such supports are relatively singular. Improvements in adaptability, lateral performance, and fast response under impact are still urgently required to meet deep mining demands. Traditional anti-impact energy-absorbing supports often reveal limitations in coping with rockburst disasters, such as insufficient energy absorption capacity and the inability to reserve enough safety space after structural compression. Based on a comprehensive analysis and summary of stress distribution patterns and support systems employed in coal mines both in China and abroad [23-25], this paper proposes a novel energy-absorbing and impact-resistant support structure. The newly proposed support adopts a yield-based energy absorption concept,

achieving energy dissipation through controlled contraction facilitated by V-shaped triggering grooves. The deformation evolution of the support was analyzed under multi-directional impact loading. The deformation and energy absorption characteristics of the most vulnerable components, including the hydraulic struts and energy-absorbing members, were investigated. Compared with traditional portal hydraulic supports, the optimized structure demonstrated significantly enhanced impact-resistant performance.

2. NUMERICAL MODEL FORMULATION

2.1 New energy-absorbing anti-impact support

Figure 1(a) shows the traditional energy-absorbing anti-impact support structure in the roadway, which can play a good supporting role when the roadway faces vertical impact, However, it does not work well against lateral impacts.

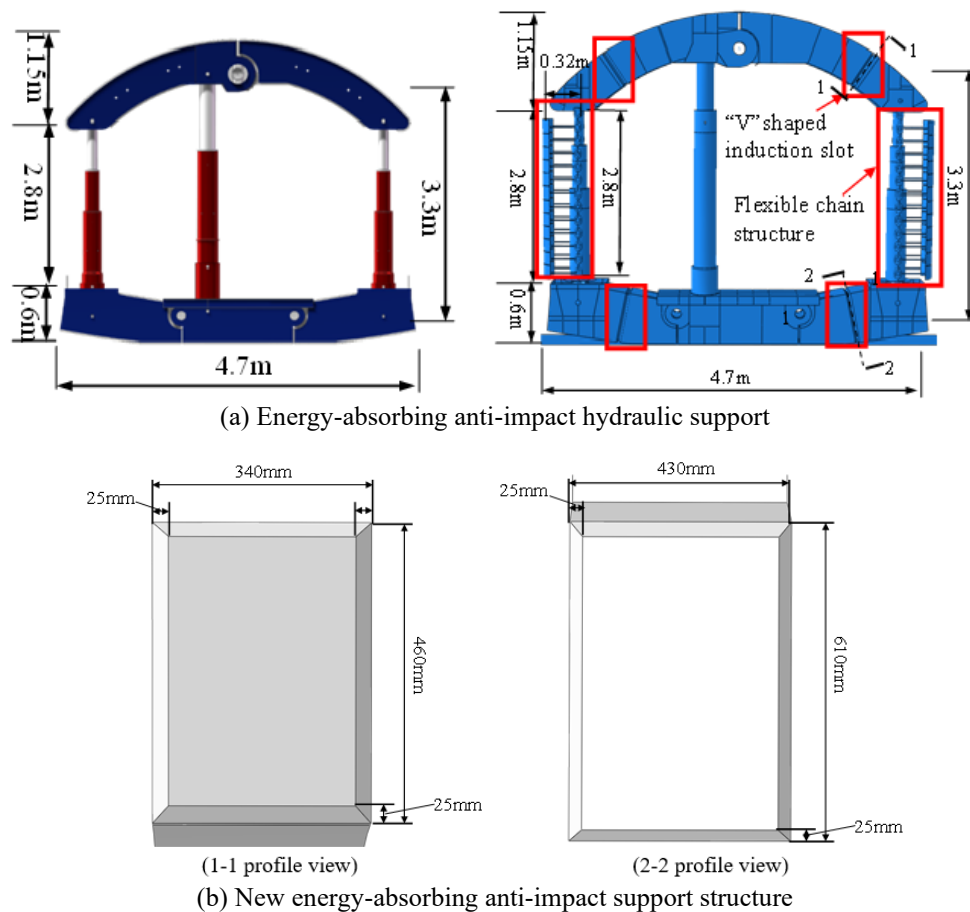


Figure 1. New energy-absorbing anti-impact support structure vs. energy-absorbing anti-shock hydraulic bracket

Based on the traditional hydraulic bracket, the flexible chain support structure is added to the outside of the columns on both sides. The flexible chain structure refers to a series of articulated links integrated on both sides of the support system. The flexible chain structure can convert the lateral impact into vertical displacement of the support. The top and bottom beams are covered with "V" shaped induced slot, to enable the beam structure to undergo certain deformation. The size of the new energy-absorbing anti-impact support structure is basically the same as that of the energy-absorbing anti-shock hydraulic bracket. Figure 1(b) shows the optimized model of the new energy-absorbing anti-impact support structure

(hereinafter collectively referred to as chain anti-impact hydraulic support).

2.2 Numerical model

In order to investigate the support performance of the chain anti-impact hydraulic support facing different impact directions, the design model is shown in Figure 2. The specific dimensions are shown in Figure 1(a).

Figure 2(a) shows setting the top rigid plate of the bracket for top impact. The impact energy is 800kJ. The vertical velocity is 4 m/s, 8 m/s, 12 m/s, 16 m/s, 20m/s and the

measurement points are set on the contact surface between the bracket and the top plate. Figure 2(b) shows the bracket on both sides of the rigid plate for lateral impact, the impact energy is set to 800kJ. As the role of the flexible chain support structure is to convert the horizontal displacement suffered into the vertical displacement of the support, the rigid plate speed is increased to 10 m/s, 15 m/s, 20 m/s, 25 m/s, 30m/s in order to make the energy-absorbing member undergo greater deformation, and the top rigid plate of the energy-absorbing member as the measurement point. The rigid plate impact time is 0.016s. Since the unilateral flexible chain structure can only affect the work of the same-side column, the impact study on different columns is to use the top plate measurement points of their same-side energy-absorbing members.

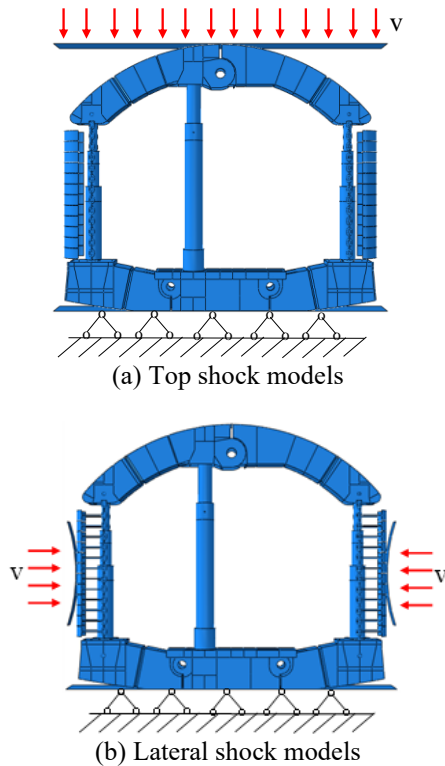


Figure 2. chain anti-impact hydraulic support model

2.3 Loading condition

The numerical model is established using ABAQUS software, and the structure is meshed with general shell element S4 at a mesh size of 30 mm, generating a total of 32,485 elements. The material used is Q785 steel, with an elastic modulus of 206 GPa, Poisson's ratio of 0.3, yield strength of 785 MPa, and density of $7.85 \times 10^3 \text{ kg/m}^3$. An ideal elastic-plastic material model was adopted in the simulation to account for the nonlinear deformation behavior of the steel under impact loading. The top and both sides of the rigid plate and the support structure are defined with general frictional contact (coefficient of 0.3), and the bottom of the support is fixed using a rigid plate.

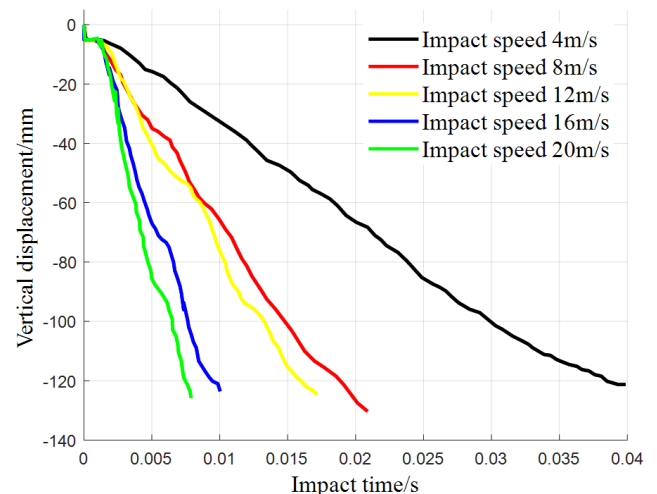
3. VERTICAL IMPACT

3.1 Deformation

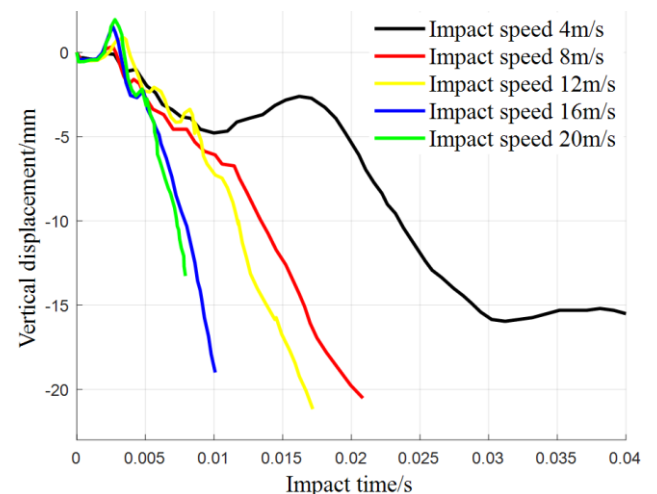
The support performance of the chain anti-impact hydraulic

support in vertical impact is investigated by impacting it with the top plate. Figure 3(a) shows the vertical displacement curve at the bottom of the middle column, with the impact speed decreasing the middle section has a tendency to slow down, i.e., the deformation of the top and bottom beams increases as the impact speed decreases; Figure 3(b) shows the vertical displacement curve of the right column, when the right column is facing the impact, it first displace upwards and then start to displace downwards; Figure 3(c) shows the vertical displacement curve of the left column, when the left column in the face of the impact first occurred upward displacement, then began to produce displacement downward, but the impact speed of 4m/s, 8m/s when the curve at the end of the rise occurred again.

Figure 4 shows the vertical displacement curves of the deformation height of the top and bottom beams of the new bracket under different impact velocities. It can be seen that when the impact speed is 4m/s, the deformation height of the top and bottom beams increases with the increase of impact time, and the deformation height of the top and bottom beams is the highest at this speed. When the impact speed is 12m/s, 16m/s, and 20m/s, there is a significant rebound in the deformation height, and as the impact speed increases, the deformation height of the bottom beam and top beam continuously decreases. This indicates that the new bracket can undergo more deformation on the top and bottom beams when facing lower impact speeds, thereby better absorbing impact energy.



(a) Middle column



(b) Right column

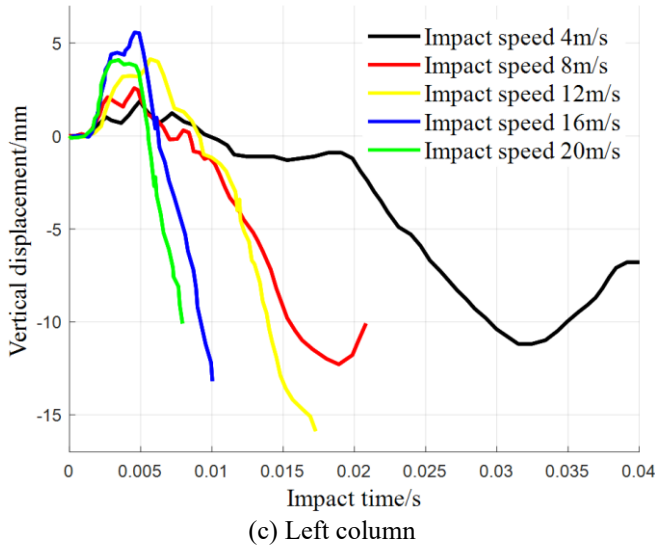


Figure 3. Vertical displacement curve at the base of the chain anti-impact hydraulic support column

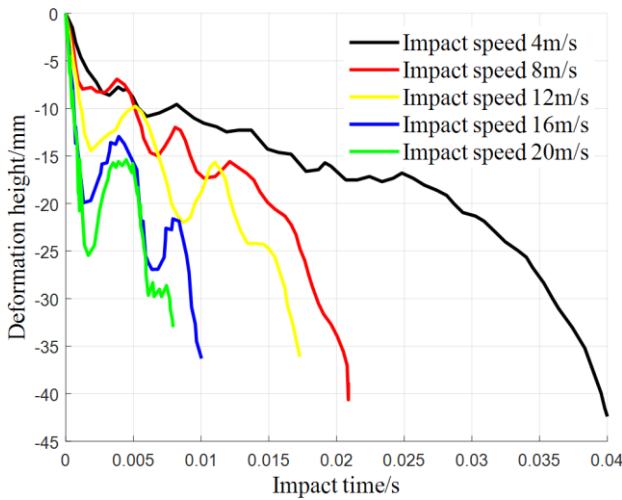


Figure 4. Vertical displacement curve of deformation height of top and bottom beams

3.2 Energy absorption

Figure 5 shows the curve of the overall plastic energy absorption of the chain anti-impact hydraulic support with the impact time, the total absorbed energy of the bracket increases continuously with the increase of impact time. With the increase of impact speed, the local plastic deformation area of the bracket increases, resulting in the increase of total absorbed energy with the increase of impact speed.

Figure 6 shows the curve of the total absorbed energy of the top and bottom beams of the bracket, from which the total absorbed energy increases with the increase of the impact speed.

For the middle energy-absorbing device, when the impact speed is 4 m/s, 8 m/s, 12 m/s, 16 m/s and 20 m/s, the energy absorbed by the device is 3.54×10^8 J, 3.74×10^8 J, 3.59×10^8 J, 3.65×10^8 J, 3.61×10^8 J, respectively. because the impact distance of the top plate is 160mm, the whole middle device has basically completed plastic deformation at the end of the impact, so its energy absorption is almost the same.

For the left energy-absorbing device, since the chain anti-impact hydraulic support bears a more concentrated load area when facing the vertical roof impact, its deformation is mainly

borne by the middle part of the bracket, so the left side energy-absorbing device does not have a large deformation, so the total energy absorbed is much lower than that of the middle.

The energy absorbed by the right device is 4.12×10^7 J, 5.53×10^7 J, 5.74×10^7 J, 5.12×10^7 J and 3.55×10^7 J, respectively, because the middle column of the chain anti-impact hydraulic support is biased to the left, the deformation of the right column is higher than the left column, so the energy absorbed by the right-side energy-absorbing device is higher than the left side one.

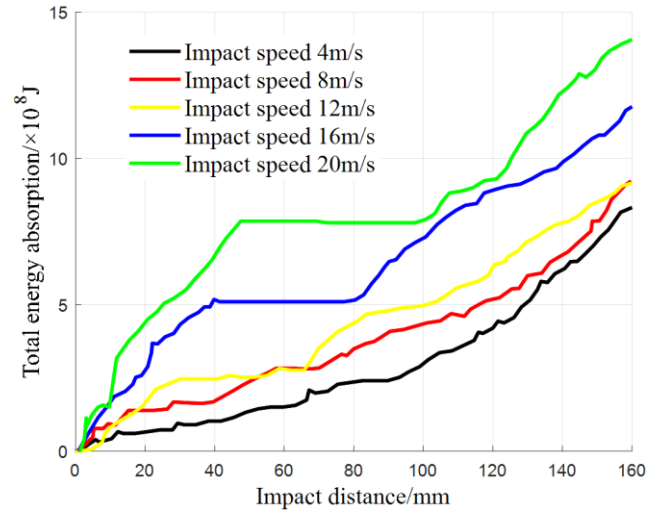


Figure 5. Plastic energy-impact time curve of the support during vertical impact

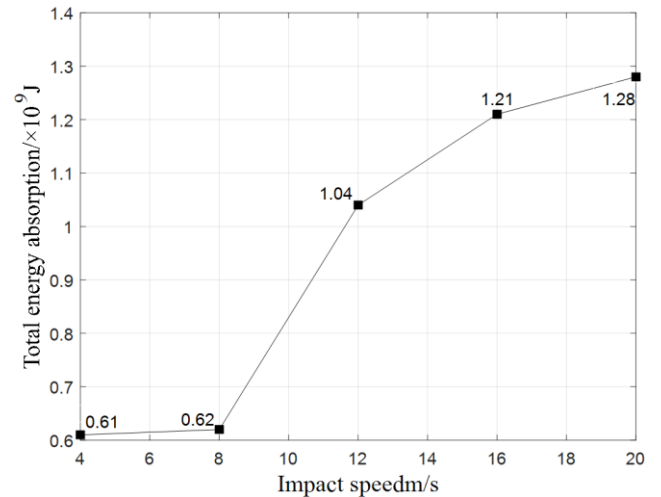


Figure 6. Curves for the total energy absorption of the top and bottom beams

4. LATERAL IMPACT

4.1 Deformation

The support performance of the chain anti-impact hydraulic support in the face of lateral impact is studied by impacting it with two lateral rigid plates. Figure 7 shows the variation curve of the chain anti-impact hydraulic support pillar sinking and base rising with time. Since the distance between the support baffle in the flexible chain structure and the pillars on both sides is 0.32m, the curve before 0.013s and 0.011s is used when the lateral impact speed is 25m/s and 30m/s,

respectively.

Figure 7(a) and (b) show the falling height curve of the middle pillar of the chain anti-impact hydraulic support and the rising height curve of the base, the impact speed is 10 m/s, 15 m/s, 20m/s when the latter section appears more obvious flat section, where the impact speed is 20m/s when the hydraulic cylinder sinks and the base rises is much higher than the other impact speed, the impact speed is 15m/s when the middle pillar also occurs a larger falling height; Figure 7(c) and (d) show the fall of the right pillar of the chain anti-impact hydraulic support, and the rising distance curve of the base respectively, the sinking of the pillar and the rising of the base at the impact speed of 25m/s is much higher than other impact speeds; Figure 7(e) and (f) show the descending height of the pillar on the left side of the chain anti-impact hydraulic support, and the rising height of the base, respectively. The sinking of the pillar and the rising trend of the base are roughly the same when the impact speed is 20 m/s, 25 m/s and 30m/s.

Figure 8 shows the compression height of the support column. From the figure, it can be seen that with the impact speed increase, the compression height of the left column increasing; with the impact speed increasing column compression height increasing, when the impact speed reached 15m/s column compression height with the impact speed increase began to reduce; with the impact speed increasing right column compression height increasing, when the impact speed reached 20m/s right column compression height with the impact speed increase began to reduce.

Combined with the analysis in Figure 7 and Figure 8, the compression height difference between the middle-column, the right column and the left column increases with the impact speed. When the impact speed is low the top and bottom beams will participate in more deformation, as the impact speed increases the beam participates in the deformation ratio decreases, i.e. Under lateral impact the energy absorbing device response priority ratio is higher than the beam response, indicates that the flexible chain support can well convert the lateral impact into the vertical impact force of the support.

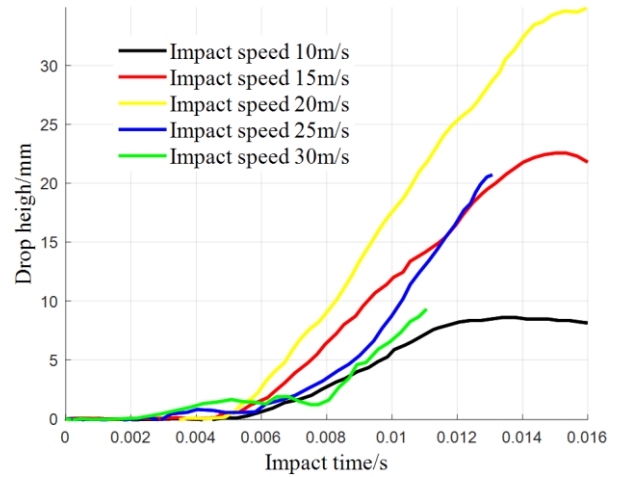
4.2 Energy absorbed

By extracting the support force of the rigid plate at the top of the energy absorbing device, the integration is done with the vertical displacement of the brace. The curve of the overall plastic energy absorption of the chain anti-impact hydraulic support as a function of the impact distance is obtained and is shown in Figure 9. As the impact speed increases the total energy absorbed by the bracket first increases and then decreases.

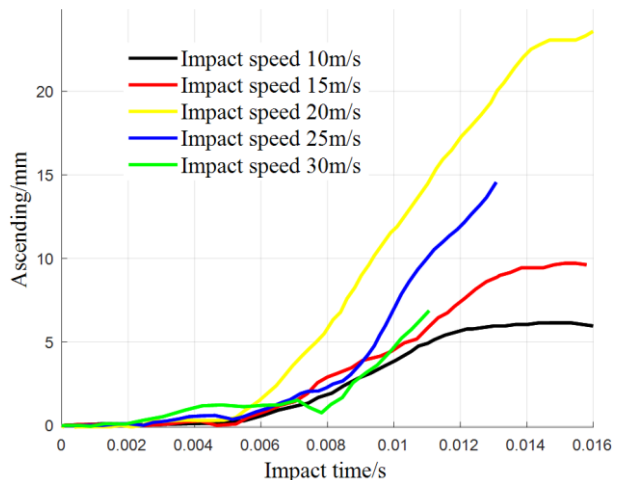
By comparing the energy absorption curves of the chain anti-impact hydraulic support for vertical impact and lateral impact, it is found that the total energy absorption of the chain anti-impact hydraulic support for lateral impact is lower than that for vertical impact, but it is in the same order of magnitude, which shows that the chain anti-impact hydraulic support can play a good supporting role in the face of lateral impact.

For the middle energy-absorbing device, the total absorbed energy increases with the impact speed firstly, when the impact speed reaches 20 m/s, the total absorbed energy starts to decrease with the impact speed; for the right energy-absorbing device, because the model impact time is 0.016s when facing the lateral impact, the lateral displacement of the side plate is only 160mm and 240mm when the impact speed

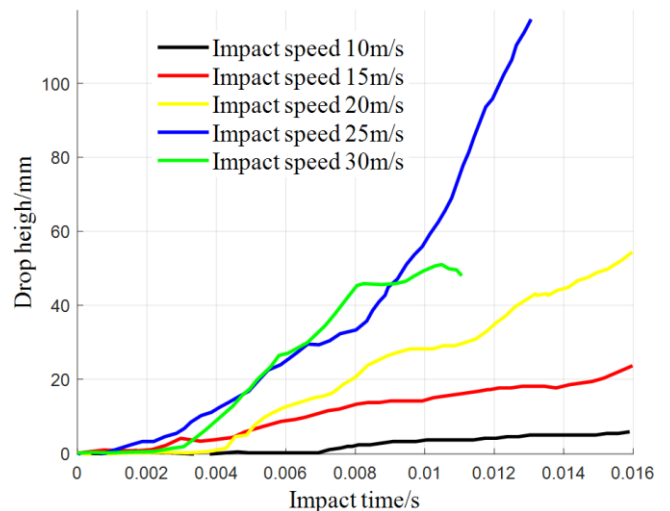
is 10 m/s and 15 m/s, so the total absorbed energy value of this device is low. The total energy absorption value of the energy-absorbing device is lower under this condition, and the maximum deformation of the side plate is completed within 0.016s when the impact speed is 20 m/s, 25 m/s and 30 m/s. The difference in the total energy absorption value of the device is not large, but it is higher than the first two conditions; because the chain anti-impact hydraulic support is impacted by both sides at the same time, the energy absorption value and trend of the left side device are basically the same as the right side.



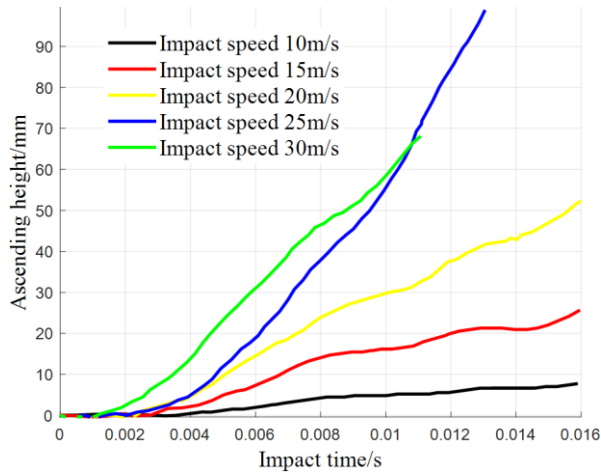
(a) Middle column sinking height-time curve



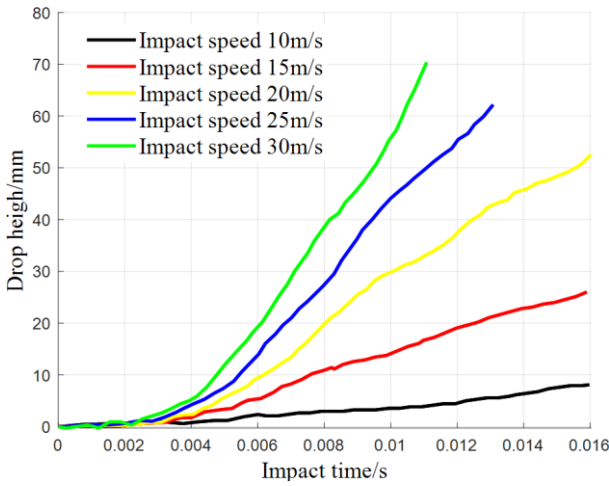
(b) Center column base Rising height-time curve



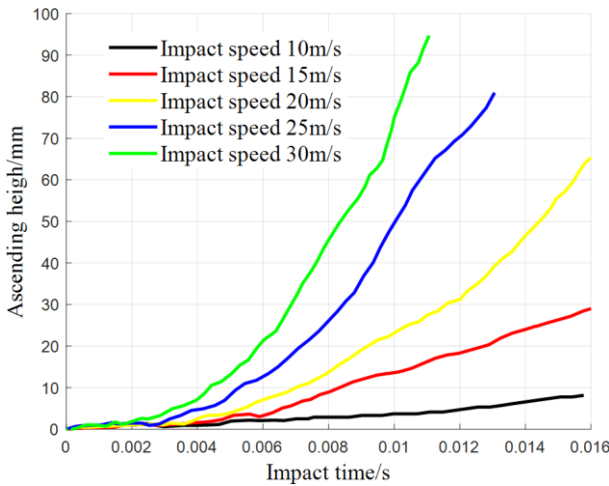
(c) Right column sinking height-time curve



(d) Right column base rise height-time curve



(e) Left column sinking height-time curve



(f) Left column base rise height-time curve

Figure 7. Height-time curves for the sinking of the chain anti-impact hydraulic support column and the rise of the base

The maximum equivalent plastic strain in the chain anti-impact hydraulic support is concentrated at the bracket-flexible support connection in the face of lower impact velocities or during normal operation. A ring base can be set up later on the bracket and used to increase the strength of the connection position between the bracket and the flexible chain structure. When the impact speed is high, the "V" shaped induced slot is deformed first, so that both sides of the "V" shaped induced slot have a relatively independent deformation

structure, which helps to protect the integrity of the overall structure of the brace.

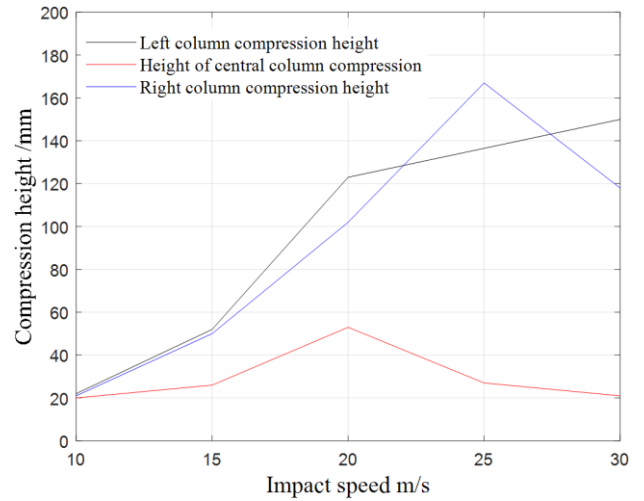


Figure 8. chain anti-impact hydraulic support strut compression height

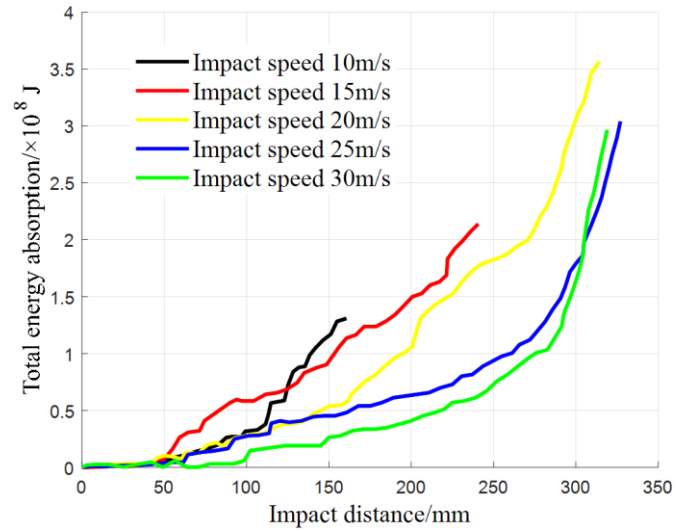
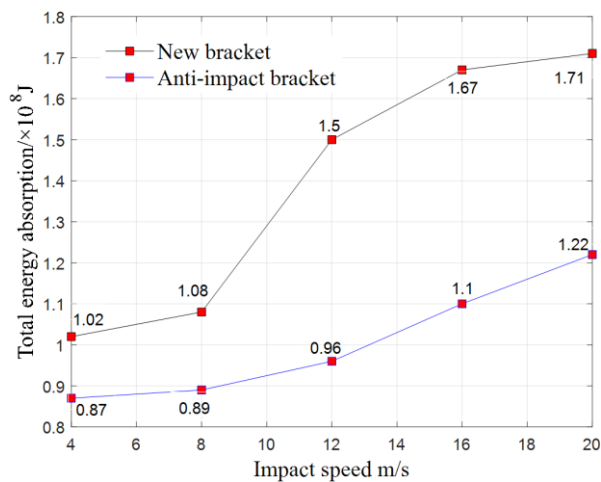


Figure 9. Total energy absorption curve of the chain anti-impact hydraulic support under lateral impact

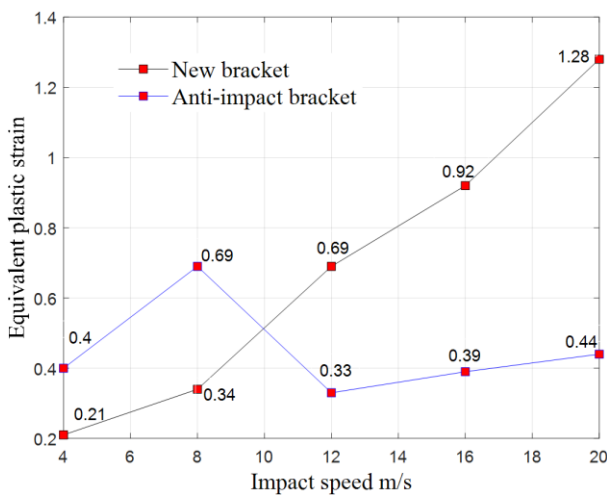
5. COMPARATIVE ANALYSIS OF NEW STENTS AND EXISTING ENERGY-ABSORBING STENTS

By comparing the traditional anti-impact bracket with the chain anti-impact hydraulic support under the same impact conditions. As shown in Figure 10(a), under the same impact velocity, the new support structure provides stable bearing capacity and energy absorption through its energy-absorbing components, working in coordination with the top and bottom beams of the support. Its absorbed energy is significantly higher than that of the impact-resistant support. Figure 10(b) shows that when the impact speed is low, the "V" shaped induced slot of the chain anti-impact hydraulic support does not produce large deformation. The deformation is mainly borne by the beam. Currently, the position of the maximum equivalent plastic strain of the 2 brackets is the same, but the equivalent plastic strain of the chain anti-impact hydraulic support is smaller. When the impact speed increases, the "V" shaped induced slot of the chain anti-impact hydraulic support

starts to deform, this structure is used as the main deformation area to protect the structural integrity of the rest of the bracket. The larger the equivalent plastic strain, the greater the extent of plastic damage in the structure, indicating that the energy absorption and displacement yielding effect of the novel support structure with the "V" shaped groove is more pronounced in mitigating the impact. In addition to its superior energy absorption performance, the new support structure also exhibits potential advantages in terms of practical application. The design maintains structural simplicity, allowing for convenient on-site installation using existing hydraulic support systems with minor modifications. The energy-absorbing components can be manufactured using conventional forming and welding techniques, which helps to control production costs. Moreover, the material selection and stress distribution indicate that the structure has favorable long-term durability under repeated impact loading, making it suitable for harsh underground environments.



(a) Total absorption energy comparison curve



(b) Equivalent plastic strain comparison curve

Figure 10. Comparison curve between the two types of brackets

5.1 Lateral impact conditions

In order to study the support effect of the chain anti-impact hydraulic support in the face of lateral impact, the models of the top and bottom beams when they are subjected to lateral impact are established respectively, as shown in Figure 11. In order to prevent the beam structure from deflecting when

subjected to lateral impact, fixed rigid plates were placed at the top and bottom of the top beam.

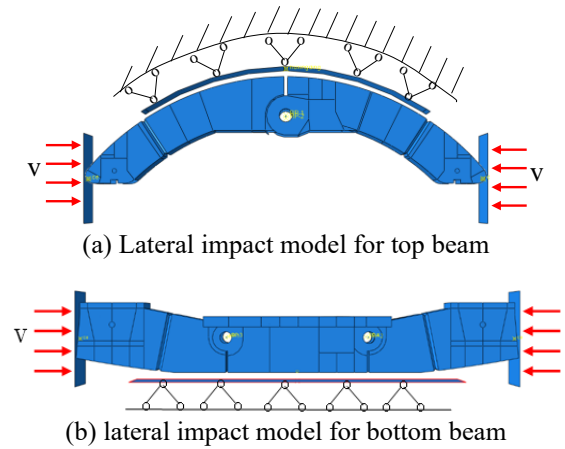


Figure 11. Numerical simulation model for lateral impact

Under transverse impact, the location of maximum equivalent plastic strains of the top and bottom beams is both in the vicinity of the "V" shaped induction slot, the maximum equivalent plastic strain of the top and bottom beam is 1.91 and 0.78; the high-stress domain of the top and bottom beams under impact is concentrated in the vicinity of the "V" shaped induced slot. "The top beam can provide a load bearing capacity of $3.07 \times 10^6 \text{ N}$ and the bottom beam can provide a load bearing capacity of $5.64 \times 10^7 \text{ N}$. The stress and equivalent plastic strain are concentrated near the "V" shaped induced slot, indicating that the "V" shaped induced slot can provide good protection to the structure deformation of the beam.

5.2 Plastic strain

When the impact speed is 4 m/s, 8 m/s, 12 m/s, 16 m/s and 20 m/s, the maximum equivalent plastic strain of the chain anti-impact hydraulic support is 0.21, 0.34, 0.69, 0.92 and 1.28 respectively. When the impact speed is 8 m/s, 16 m/s and 20 m/s, the location of the highest equivalent plastic strain of the chain anti-impact hydraulic support is at the "V" shaped induced slot on the right side of the top beam, which indicates that the top beam connection location is the most vulnerable position in the face of vertical impact, so the subsequent thickening treatment should be carried out to increase the strength of the top beam connection location. At the same time, the "V" shaped induced slot of the chain anti-impact hydraulic support can protect the structural integrity of the top beam to a certain extent.

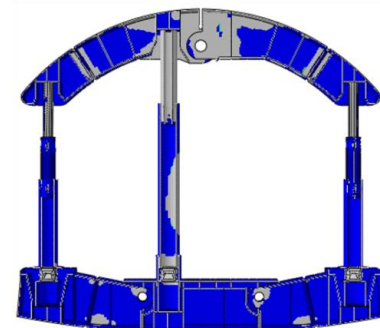


Figure 12. Cloud view of the yield position of the new bracket

As there is no major change in the overall location where the yielding of the chain anti-impact hydraulic support occurs at different impact velocities, the equivalent plastic strain cloud diagram of the chain anti-impact hydraulic support at an impact speed of 20m/s is taken as an example, as shown in Figure 12. For easy observation, the flexible chain structure is hidden in Figure 12, it can be found that the equivalent plastic strain area is mainly concentrated in the middle of the top beam, the upper part of the left and right-side hydraulic cylinders, the upper part of the central hydraulic cylinder and the middle, the above locations are the main load-bearing locations of the energy-absorbing bracket. The gray area in the figure shows the plastic deformation area of the bracket.

6. CONCLUSIONS

(1) When the chain anti-impact hydraulic support faces the top impact with different impact velocities, the equivalent plastic strain position appears at the middle joint of the top beam and the "V" shaped induced slot, indicating that the central connection position of the top beam is the most vulnerable under vertical impact. Subsequent structural optimization should reinforce this critical region. This localized damage control mechanism plays a significant role in mitigating structural failure under concentrated dynamic loads, which is particularly important in mining scenarios prone to rockburst.

(2) The hydraulic columns did not exhibit any strain concentration during the vertical impact process, indicating that the hydraulic cylinders can safely endure the response time of the safety valve under the protection of the energy-absorbing mechanism. The vertical displacement of the middle column was larger than that of the two side columns, suggesting that the "V" shaped induced slot provides partial isolation of rectangular deformation in the beam structure. This buffering effect helps to delay the propagation of deformation and reduce peak stress transmission, offering an advantage in absorbing the initial energy surge during a rockburst event.

(3) As vertical impact velocity increases, the impact energy absorbed by the new support structure and its top and bottom beams continuously increases. This indicates that higher impact velocity leads to larger yielding zones in the beam steel plates. Meanwhile, the deformation height of the top beam continuously decreases with increasing impact velocity, and the deformation of the "V" shaped induced slot is smaller under higher velocities and larger under lower velocities. This suggests that the slot exhibits a certain response speed to vertical impact. Such responsiveness demonstrates the capability of the induced slot design to rapidly activate energy dissipation mechanisms, enhancing support performance during early-stage rockburst shockwaves.

(4) Compared with traditional hydraulic supports, the V-shaped slot effectively divides the support structure and provides deformation flexibility for the beam, allowing it to cooperate with energy-absorbing elements to mitigate impact loads. It significantly reduces the effect of localized deformation on other parts of the structure. Thus, the optimized chain anti-impact hydraulic support outperforms conventional support systems under vertical impact. This structural zoning strategy improves the internal force distribution and containment of failure zones, providing enhanced protection against asymmetric failure modes

typically triggered by rockburst impacts.

(5) Under lateral impact conditions, the equivalent plastic strain is mainly concentrated at the connection between the flexible chain and the main support under low-speed impact. A connection base should be added at this location. When subjected to high-speed impacts, the strain is primarily concentrated around the "V" shaped induced slot, suggesting that the slot can effectively respond to lateral impacts. This ensures relatively independent deformation between the two sides of the support and reduces the mutual influence of bilateral deformation on the overall structural integrity. This lateral adaptability is essential in preventing structural collapse during sudden asymmetric disturbances caused by rockburst along roadway sides.

(6) Through the analysis of column displacement and energy dissipation under various impact velocities, it was found that the flexible chain support component of the chain anti-impact hydraulic support performs well in lateral load resistance. Although its bearing capacity and total energy absorption are slightly weaker under lateral impacts than under vertical impacts, it still provides effective lateral support. Moreover, the vertical displacement transmitted to the center column from the lateral beam structure varies with impact velocity, with lower transmission efficiency at both higher and lower speeds. This characteristic filtering effect enables selective damping of lateral impact forces, thereby enhancing the structural resilience of the support system during sudden seismic energy releases.

(7) This study proposes a new type of anti-impact support and evaluates its performance under vertical and lateral impact conditions. However, the current analysis is based on simplified assumptions, such as fixed impact velocities and homogeneous material properties, which do not fully capture the complexity of actual underground environments. These limitations may affect the applicability of the results to real mining scenarios. Future work should introduce variable impact conditions, consider material heterogeneity, and assess long-term behavior under cyclic loading.

(8) Although the proposed support structure demonstrates favorable mechanical performance under dynamic loading, its application in actual underground engineering requires further observation. The overall configuration of the new anti-impact support is similar in size and form to conventional impact-resistant supports; however, due to its structural particularities, certain challenges may arise during practical manufacturing. Moreover, underground roadways often present complex conditions, and even traditional energy-absorbing supports can encounter compatibility issues, which in turn increases the overall economic cost. Future research may focus on optimizing the structural design while maintaining support strength, aiming to improve feasibility without compromising performance.

Reference

- [1] Basnet, P.M.S., Jin, A., Mahtab, S. (2024). Developing an explainable rockburst risk prediction method using monitored microseismicity based on interpretable machine learning approach. *Acta Geophysica*, 72(4): 2597-2618. <https://doi.org/10.1007/s11600-024-01338-y>
- [2] Carranza-Torres, C., Diederichs, M. (2009). Mechanical analysis of circular liners with particular reference to composite supports. For example, liners consisting of

- shotcrete and steel sets. *Tunnelling and Underground Space Technology*, 24(5): 506-532. <https://doi.org/10.1016/j.tust.2009.02.001>
- [3] Carranza-Torres, C. (2004). Elasto-plastic solution of tunnel problems using the generalized form of the Hoek-Brown failure criterion. *International Journal of Rock Mechanics and Mining Sciences*, 41(S1): 629-639. <https://doi.org/10.1016/j.ijrmms.2004.03.111>
- [4] Salehi, B., Golshani, A., Rostami, J., Schneider-Muntau, B. (2024). Simulation of complex support systems for large span tunnels: Investigation on support interferences and effects of constitutive models. *KSCE Journal of Civil Engineering*, 28(11): 5309-5324. <https://doi.org/10.1007/s12205-024-5581-4>
- [5] Pan, Y., Xiao, Y., Luo, H., Wang, G., Shi, T. (2023). Study on safety of rockburst mine. *Journal of China Coal Society*, 48(5): 1846-1860. <https://doi.org/10.13225/j.cnki.jccs.2023.0294>
- [6] Qi, Q.X., Zhao, S.K., Li, H.T., Qin, K. (2020). Several key problems of coal bump prevention and control in China's coal mines. *Safety in Coal Mines*, 51(10): 135-143. <https://doi.org/10.13347/j.cnki.mkaq.2020.10.021>
- [7] Xie, H.P., Gao, F., Ju, Y., Ge, S.R., et al. (2017). Theoretical and technological conception of the fluidization mining for deep coal resources. *Journal of China Coal Society*, 42(3): 547-556. <https://doi.org/10.13225/j.cnki.jccs.2019.6038>
- [8] Qi, Q., Pan, Y., Shu, L., Li, H., et al. (2018). Theory and technical framework of prevention and control with different sources in multi-scales for coal and rock dynamic disasters in deep mining of coal mines. *Journal of China Coal Society*, 43(7): 1801-1810. <https://doi.org/10.13225/j.cnki.jccs.2018.0660>
- [9] Tan, Y., Guo, W., Xin, H., Zhao, T., Yu, F., Liu, X. (2019). Key technology of rockburst monitoring and control in deep coal mining. *Journal of China Coal Society*, 44(1): 160-172. <https://doi.org/10.13225/j.cnki.jccs.2019.5088>
- [10] Terron-Almenara, J., Panthi, K.K. (2025). Analysis of plastic deformations for tunnel support design in weak flysch rock mass of a hydropower tunnel in Central Albania. *Rock Mechanics and Rock Engineering*. <https://doi.org/10.1007/s00603-025-04545-1>
- [11] Askaripour, M., Saeidi, A., Rouleau, A., Mercier-Langevin, P. (2022). Rockburst in underground excavations: A review of mechanism, classification, and prediction methods. *Underground Space*, 7(4): 577-607. <https://doi.org/10.1016/j.undsp.2021.11.008>
- [12] Qi, Q.X., Li, Y.Z., Zhao, S.K., Zhang, N., Zheng, W., Li, H., Li, H.Y. (2019). Seventy years development of coal mine rockburst in China: Establishment and consideration of theory and technology system. *Coal Science and Technology*, 47(9): 1-40. <https://doi.org/10.13199/j.cnki.cst.2019.09.001>
- [13] Qi, Q., Pan, Y., Li, H., Jiang, D., et al. (2020). Theoretical basis and key technology of prevention and control of coal-rock dynamic disasters in deep coal mining. *Journal of China Coal Society*, 45(5): 1567-1584. <https://doi.org/10.13225/j.cnki.jccs.DY20.0453>
- [14] Le, Q.P., Dao, V.C. (2022). Roof condition characteristics affecting the stability of coal pillars and retained roadway. In *International Conference on Geo-Spatial Technologies and Earth Resources*, Hanoi, Vietnam, pp. 463-477. https://doi.org/10.1007/978-3-031-20463-0_29
- [15] Jilo, N.Z., Assefa, S.M., Assefa, E. (2024). Numerical analysis of underground tunnel deformation: A case study of Midroc Lega-Dembi gold mine. *Scientific Reports*, 14(1): 7964. <https://doi.org/10.1038/s41598-024-57621-x>
- [16] Bashir, M.S., Khushnood, S., Nizam, L.A., Javaid, M.Y., Usman, M., Rashid, M.M. (2024). Fretting wear analysis of flexible vibrating tube interacting with the support plate in low-speed water tunnel. *Journal of Vibration Engineering & Technologies*, 12(2): 2409-2424. <https://doi.org/10.1007/s42417-023-00987-5>
- [17] Boukarm, R., Fredj, M., Saadoun, A. (2024). Performance evaluation of tunnel support system in jointed rock mass by numerical simulation: A case study. *KSCE Journal of Civil Engineering*, 28(4): 1534-1545. <https://doi.org/10.1007/s12205-024-0529-2>
- [18] Gangwar, A., Handa, S., Kumar, J., Singh, M., Dwivedi, R.D. (2025). A case study of tunnel stability in quaternary deposits using pipe-roof supports. *Indian Geotechnical Journal*, 55(1): 426-442. <https://doi.org/10.1007/s40098-024-00892-y>
- [19] Marinos, V., Goricki, A., Malandrakis, E. (2019). Determining the principles of tunnel support based on the engineering geological behaviour types: Example of a tunnel in tectonically disturbed heterogeneous rock in Serbia. *Bulletin of Engineering Geology and the Environment*, 78(4): 2887-2902. <https://doi.org/10.1007/s10064-018-1277-7>
- [20] Vardoulakis, I. (1984). Rock bursting as a surface instability phenomenon. *International Journal of Rock Mechanics and Mining Sciences & Geomechanics Abstracts*, 21(3): 137-144. [https://doi.org/10.1016/0148-9062\(84\)91531-6](https://doi.org/10.1016/0148-9062(84)91531-6)
- [21] Ma, X., Pan, Y., Zhang, J., Xiao, Y. (2018). Design and performance research on core energy absorption component of anti-impact support. *Journal of China Coal Society*, 43: 1171-1178. <https://doi.org/10.13225/j.cnki.jccs.2017.0693>
- [22] Pan, Y.S., Xiao, Y.H., Li, Z.H., Wang, K.X. (2014). Study of tunnel support theory of rockburst in coal mine and its application. *Journal of China Coal Society*, 39(2): 222-228. <https://doi.org/10.13225/j.cnki.jccs.2013.2015>
- [23] Azad, M.A., Naithani, A.K., Shekhar, S., Ahmad, S., Singh, S.K. (2023). Tunnel support validation using numerical modelling: A case study from NW, Himalaya, India. *Geotechnical and Geological Engineering*, 41(7): 4335-4349. <https://doi.org/10.1007/s10706-023-02506-5>
- [24] Basarir, H. (2006). Engineering geological studies and tunnel support design at Sulakyurt dam site, Turkey. *Engineering Geology*, 86(4): 225-237. <https://doi.org/10.1016/j.enggeo.2006.05.003>
- [25] Panthi, K.K., Shrestha, P.K. (2018). Estimating tunnel strain in the weak and schistose rock mass influenced by stress anisotropy: An evaluation based on three tunnel cases from Nepal. *Rock Mechanics and Rock Engineering*, 51: 1823-1838. <https://doi.org/10.1007/s00603-018-1448-7>